IEEE Photonics Journal
An IEEE Photonics Society Publication



# The Study on the Droop Effect in the InGaN/AlGaInN MQWs With Lattice-Matched AlGaN/InGaN Superlattices Barrier by Highly Excited Photoluminescence Measurement

Volume 10, Number 2, April 2018

Fulong Jiang
Yaying Liu
Menghan Liu
Ningze Zhuo
Peng Gao
Huajie Fang
Peng Chen
Bin Liu
Xiangqian Xiu
Zili Xie
Ping Han
Yi Shi
Rong Zhang
Youdou Zheng

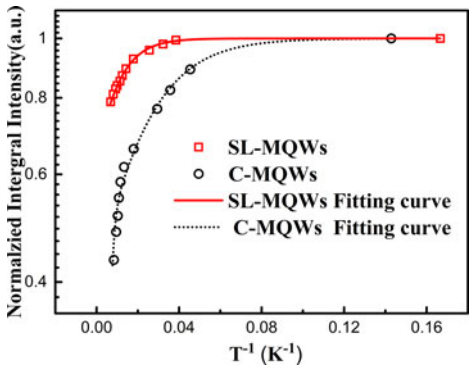


DOI: 10.1109/JPHOT.2018.2820692
1943-0655 

# The Study on the Droop Effect in the InGaN/AlGaInN MQWs With Lattice-Matched AlGaN/InGaN Superlattices Barrier by Highly Excited Photoluminescence Measurement

**Fulong Jiang,[1] Yaying Liu,[1] Menghan Liu,[1] Ningze Zhuo,[1] Peng Gao,[1] Huajie Fang,[1] Peng Chen,[1,2] Bin Liu,[1] Xiangqian Xiu,[1] Zili Xie,[1] Ping Han,[1] Yi Shi,[1] Rong Zhang,[1] and Youdou Zheng[1]**

[1]Key Laboratory of Advanced Photonic and Electronic Materials, School of Electronic Science and Engineering, Nanjing University, Nanjing 210093, China.
[2]Nanjing University Institute of Optoelectronics at Yangzhou, Yangzhou 225009, China.

*DOI:10.1109/JPHOT.2018.2820692*


Manuscript received March 12, 2018; accepted March 26, 2018. Date of publication March 29, 2018; date of current version April 11, 2018. This work was supported by the National Key R&D program of China under Grant 2016YFB0400602. Corresponding author: Peng Chen (e-mail: pchen@nju.edu.cn).

**Abstract:** We have fabricated the InGaN/AlGaInN multiple quantum wells with lattice-matched AlGaN/InGaN superlattices barriers (SL-MQWs). The lattice-matched superlattices promote the formation of the high-quality MQWs and eliminate the large polarization electric field. Highly excited photoluminescence measurement is performed by Ti-sapphire pulse laser with the maximal carrier density of $10^{20}$ $cm^{-3}$. Under such high carrier density, the conventional InGaN/GaN MQWs (C-MQWs) have an additional nonradiative loss of carriers and suffer from the efficiency droop effect, while slight droop behavior is observed in the SL-MQWs sample. The results show that the substitution of AlGaN/InGaN superlattices as quantum barriers can effectively suppress the droop behavior at highly excited condition.

**Index Terms:** InGaN, Multiple Quantum Wells, polarization, efficiency droop.

## 1. Introduction

Group Iii-Nitrides have been achieved great success in the field of solid state lighting due to the high internal quantum efficiency and the adjustable bandgap varying with the alloy composition [1], [2]. Despite these great successes, approaching the high-power devices and increasing the luminosity of light emitting diodes (LED) is still challenging [3], [4]. The most significant issue is the efficiency droop – the decrease in quantum efficiency with increasing drive current. Intense researches have been performed to investigate the physical mechanisms of the efficiency droop. Defect-related mechanisms, Auger recombination, electron leakage and carriers delocalization *et al.* have been proposed to be responsible for the efficiency droop [5], [6], [7]. One promising way to overcome the fundamental challenges is to grow InGaN/GaN multiple quantum wells (MQWs) along a semi- or non-polar direction which can reduce or eliminate the internal electric fields. And the AlGaInN quarternary alloy grown on *c*-sapphire is also an effective way to reduce the polarization filed in the

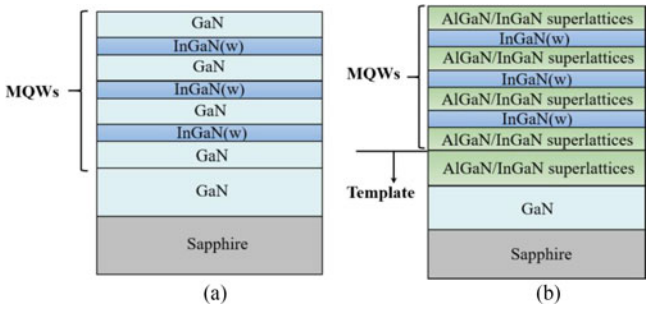


Fig. 1. The Structural schematic of the (a) C-MQWs and the (b) SL-MQWs.

MQWs [8], [9]. The recent researches focus on the weaken of the polarization induced built-in field and suppress the efficiency droop successfully [10], [11]. However, the latest research by Davies has shown that both the polar and non-polar InGaN/GaN quantum wells structures suffer from the efficiency droop while carrier density exceeds $7 \times 10^{11}$ cm$^{-2}$ pulse$^{-1}$ QW$^{-1}$ [12]. Especially, a transition with rapidly decaying constant (ps) at higher energy side of emission spectrum is recommend as the one of the origins for efficiency droop at highly excited condition [13]. However, the generally acknowledged origin of droop is still under dispute, particularly in the non-polar InGaN/GaN MQWs.

In this paper, we fabricate polarization matched InGaN/AlInGaN MQWs, in which the conventional GaN barriers are replaced by AlGaN/InGaN superlattices. The completely coherent InGaN/AlInGaN MQWs is obtained with greatly suppression of built-in electric field. The highly excited photoluminescence (PL) measurement is performed compared with that of conventional InGaN/GaN MQWs. We have investigated the recombination mechanism at highly excited condition by comparing the conventional InGaN/GaN MQWs and the InGaN/AlInGaN MQWs with lattice-matched AlGaN/InGaN superlattices barrier. The result shows that the use of lattice-matched AlGaN/InGaN superlattices barrier layer can effectively improves the materials quality and suppress the efficiency droop.

## 2. Experimental Details

The conventional MQWs (C-MQWs) and InGaN/AlGaInN MQWs (SL-MQWs) are grown on the *c*-plane sapphire by Metal-Organic Chemical Vapor Deposition reactor (MOCVD). Fig. 1 is the schematic diagram of the C-MQWs and SL-MQWs respectively. For the SL-MQWs sample, 25-nm-thick GaN buffer layer is grown on c-plane of sapphire substrate, followed with 1.5-$\mu$m GaN layer. On the top of the GaN layer, about 80-nm-thick AlInGaN layer is deposited for relaxing the lattice constant. The 80-nm-thick AlInGaN layer consist of twenty-period AlGaN/InGaN superlattices, in which each InGaN or AlGaN layer is about 2 nm. On the AlInGaN superlattices layer, three-period InGaN/AlInGaN MQWs is deposited. Each AlInGaN barrier consists of 3-period AlGaN/InGaN superlattices. By adjusting the component of In and Al in the superlattice, the equivalent lattice constant of the AlGaN/InGaN superlattice can well matches with that of the InGaN well layer in the MQWs. X'pert Epitaxy software is used to simulate the composition of Al and In element of the superlattices structure. The result shows that the composition of Al and In are 13.6% and 3.1%, respectively. We have performed the PL measurement to the AlGaN/InGaN superlattices structure. The emission wavelength of the AlGaN/InGaN superlattcies is located at 371 nm. For comparison with the polarized MQWs, the conventional three-period InGaN/GaN MQWs are grown by MOCVD with the similar growth condition.

We tested the surface morphology of the two samples by scanning electron microscopy (SEM). The photoluminescence spectra were obtained by using Ti-sapphire pulse laser as the excitation source. The excited wavelength is tuned to 375 nm to generate carriers in the Quantum wells directly. The maximum time averaged excitation density is 34 kW/cm$^2$ with a pulse width of 170 fs and a repetition rate of 78 MHz [12]. The pulse duration is shorter than the carrier recombination

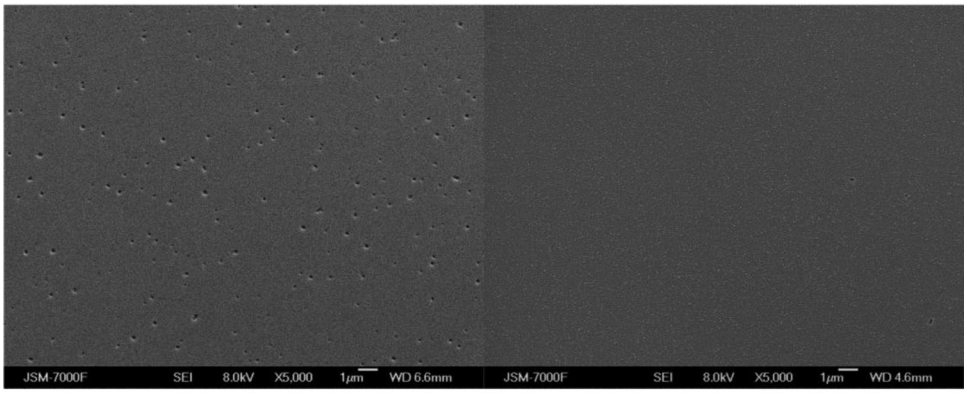


(a) (b)

Fig. 2. The SEM image of the (a) C-MQWs and the (b) SL-MQWs.

lifetimes, therefore the peak carrier concentration in the MQWs is determined by the density of the excitation source. Assuming that the absorption coefficient is $5 \times 10^4\,cm^{-1}$, a single pulse excitation leads to an estimated maximum carrier density of $\sim 10^{20}\,cm^{-3}$.

## 3. Results and Discussions

The SEM images of C-MQWs and SL-MQWs are shown in Fig. 2(a) and (b) respectively. V-pit, a common defect formed in the InGaN/GaN QWs at the end of threading dislocation, is found on the surfaces of both samples. By calculation, the defect density of the C-MQWs is about $5.1 \times 10^8\,cm^{-2}$. In the C-MQWs, the InGaN well layers are clamped up and down by the GaN barriers. And the growth temperature of MQWs is 800 °C due to the low binding energy of In-N. Hence, the misfit strain and low surface mobility of adatoms tend to forming V-pits at the apex of the threading dislocation [14], [15]. However, in the SL-MQWs, the barriers are replaced by the AlGaN/InGaN superlattices, which the equivalent lattice well matchs the InGaN wells. The driving force for the formation of V-pits is almost eliminated [16]. As shown in Fig. 2(b), the defect density of the SL-MQWs is about $4.7 \times 10^5\,cm^{-2}$, which is three orders of magnitude less than that of C-MQWs.

As shown in the Fig. 3(a) and (b), the emission wavelength of the C-MQWs and the SL-MQWs are 465 nm and 430 nm respectively. The peak position of C-MQWs has a blueshift of 19 nm with the increasing carrier density, while the peak position of SL-MQWs only has a slightly swing within 2 nm. We attribute the large blueshift of C-MQWs to the screen of polarization field induced QCSE by photo-excited carriers and the band billing effect. For SL-MQWs, the stability of peak position indicates that the piezoelectric field is almost eliminated. The slightly swing within 2 nm might be the competition result of band filling effect and band-gap renormalization [17]. As the carrier density increase to $2 \times 10^{18}\,cm^{-3}$, the electron-hole plasma renormalize the band-gap energy and result in the emission redshift [18], [19]. When the carrier density exceeds $10^{18}\,cm^{-3}$, the band filling effect overtakes the band-gap renormalization, resulting in the emission blueshift.

The FWHM of the two samples also exhibit different trends with increasing carrier density. The FWHM value of the SL-MQWs is overall less than that of the C-MQWs which means a good in-plane uniformity in the SL-MQWs. For the C-MQWs, the huge built-in electric field incline the energy band of the quantum well. The Indium fluctuation and the tilted energy band expand the energy level for the carriers to radiative recombination. As the carrier density increases to $8 \times 10^{17}\,cm^{-3}$, the screening of polarization field makes the slope of the energy band smaller and result in the decrement of FWHM. As the carrier density increase from $8 \times 10^{17}\,cm^{-3}$ to $8 \times 10^{18}\,cm^{-3}$, the band filling effect balances the screening effect, making the FWHM value remain constant. The polarized electric field is shielded and the energy band is flattened until the carrier density reaches $8 \times 10^{18}\,cm^{-3}$. Combined with the shift value of emission wavelength, the polarized electric field and polarized charge density for the C-MQWs are calculated to be 0.2 MV/cm and $2.4 \times 10^{12}\,cm^{-2}$ respectively.

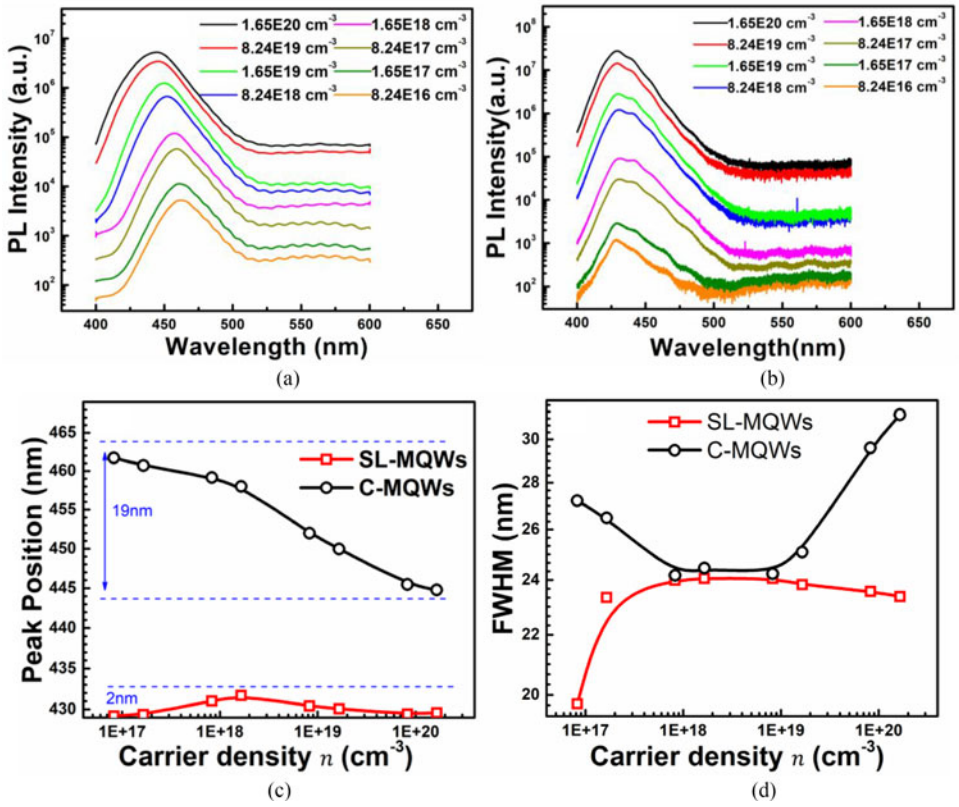


Fig. 3. The photoluminescence spectra of the C-MQWs sample (a), the SL-MQWs sample (b) The peak energy (c), and the FWHM (d), versus carrier density are plotted at logarithmic coordinates.

When the carrier density exceeds $10^{19}$ cm$^{-3}$, the FWHM value of the C-MQWs increase while that of the SL-MQWs remain constant, as shown in Fig. 3(d). It should be noted that the increment of the PL FWHM is correlated with the onset of droop which arising from an extra emission component involving delocalized carriers [13]. Actually, the droop behavior is much significant in the C-MQWs rather than the SL-MQWs when carrier density exceeds $10^{19}$ cm$^{-3}$. We ascribe the absence of the droop behavior to the substitution of AlGaN/InGaN superlattices as quantum barriers. The specific analysis is shown as below.

All of the above phenomena show that the polarization effect in SL-MQWs have been well eliminated by using lattice matched AlGaN/InGaN superlattices. In the following section, we will discuss plot of the internal quantum efficiency ($\eta_{\text{int}}$) vs. the carrier density *n,* as shown in the Fig. 4. Since the excitation wavelength is at 375 nm, the laser can only be absorbed by the three-period InGaN well layers (9 nm) for the two samples. Carriers are directly generated in the InGaN wells and there is no need to consider the capture process of carriers by quantum wells. Therefore, the recombination channel of carriers can be analyzed by means of $An + Bn^2 + Cn^3 + kn^m$ [5], [12], [20], where A*n* represents the Shockly-Read-Hall nonradiative recombination, B$n^2$ represents the radiative recombination and C$n^3$ represents the Auger recombination. Especially, $kn^m$ represents a kind of nonradiative loss mechanism associated with carrier delocalization. Based on the integral PL intensity versus carrier density measurement, the $\eta_{\text{int}}$ can be deduced through the relation, $\eta_{\text{int}} = Bn^2/An + Bn^2 + Cn^3 + kn^m$. And the integral PL intensity (*I*) and excitation density (kW/cm$^2$) are proportional to the radiative recombination ($Bn^2$) and carrier density (*n*), respectively. Therefore, the ratio of *I* and excitation density (kW/cm$^2$) reveal the relatively variation tendency of the $\eta_{\text{int}}$ with the increasing carrier density at 300 K, as shown in Fig. 4. The absolute value of the $\eta_{\text{int}}$ for the two sample are obtained through the temperature-dependent PL measurement which is performed by

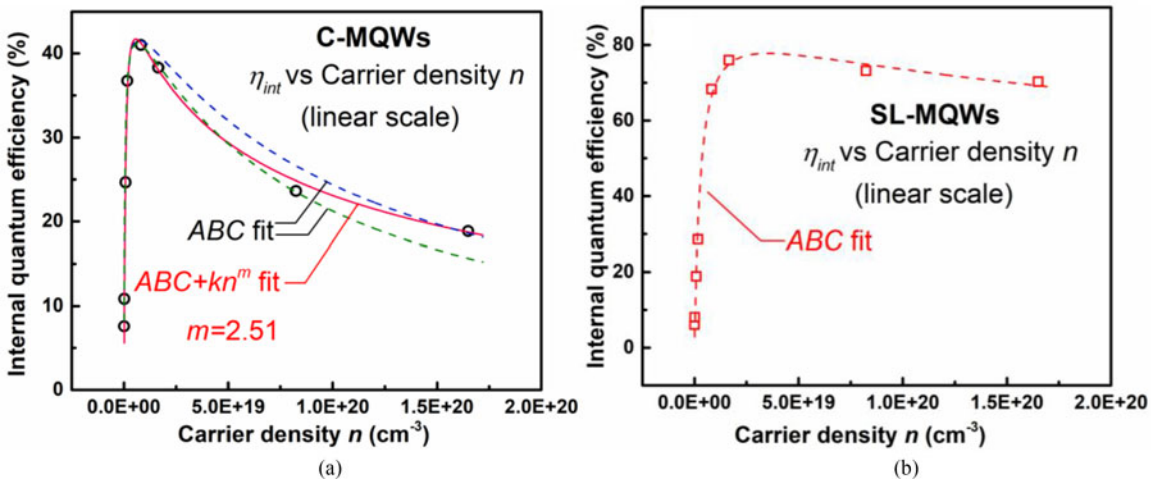


Fig. 4. The internal quantum efficiency of the C-MQWs (a) and SL-MQWs (b), the dash lines are the fitting curve by adopting the ABC model, and the solid line is fitted by adopting the ABC + $kn^m$ model.

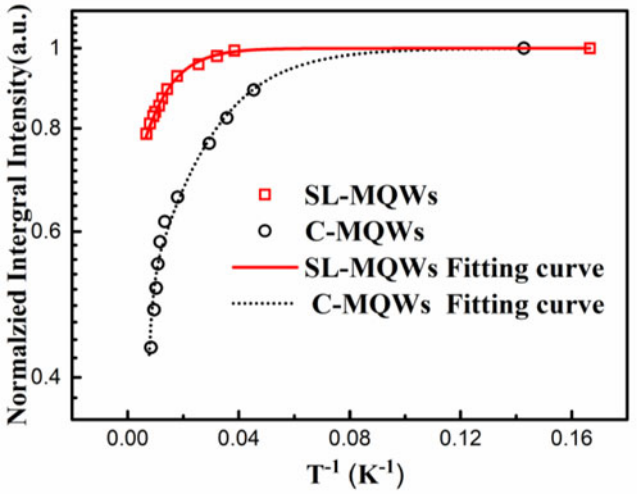


Fig. 5. Arrhenius plots of integrated PL intensity for the SL-MQWs and C-MQWs.

a closed cycle cryostat. The normalized integral PL intensity versus the reciprocal of temperature is plotted in Fig. 5. The integral PL intensity at 6 K for the two sample are used as a benchmark to calculate the value of the $\eta_{\text{int}}$. Based on these foundations, the peak $\eta_{\text{int}}$ of the C-MQWs and SL-MQWs are calculated to be 42% and 78%, respectively.

Fig. 4 shows the $\eta_{\text{int}}$ vs. carrier density $n$ with linear coordinates. For the C-MQWs, the peak of the $\eta_{\text{int}}$ is 42%, corresponding to the carrier density of $\sim 5.1 \times 10^{18}\,\text{cm}^{-3}$, which is close to observed carrier density at the maximum peak efficiency of *c*-plane InGaN/GaN MQWs LEDs. With the carrier density keep increasing, the $\eta_{\text{int}}$ decrease from 42% to 18%, as shown in Fig. 4(a). Fitting the date with ABC model, we find a good fit can be obtained for the efficiency curve at carrier density below that of the peak efficiency shown in Fig. 4(a) with two dash lines. However, the fit with ABC model fails to keep pace with the decline at higher carrier density, especially the carrier density $n$ exceeds $8 \times 10^{18}\,\text{cm}^{-3}$. We can't obtain a suitable Auger coefficient to fit with the experiment date. The solid line in Fig. 4(a) shows the fitting curve by adopting $ABC + kn^{\text{m}}$ model with $m = 2.51$, which can well fit with the experiment date both under low and high carrier density. The additional nonradiative losses, with 2.51-order of the carrier density, may associate with carrier delocalization related nonradiative loss channel. For the SL-MQWs, as shown in the Fig. 4(b), the

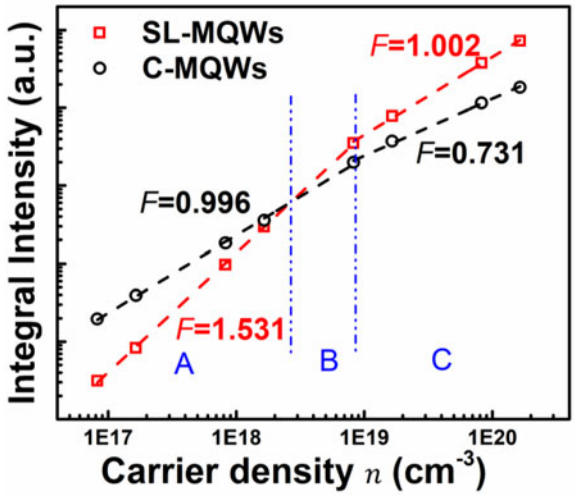


Fig. 6. The integral intensity of two samples varies with carrier density with logarithmic coordinates.

peak efficiency of the SL-MQWs is 79%. While the carrier density exceed $10^{19}$ $cm^{-3}$, the efficiency of the SL-MQWs has slightly decrement. The plot of the $\eta_{int}$ of the SL-MQWs can be well fitted with ABC model, shown in the Fig. 4(b) with solid line. The Auger recombination coefficient is fitted to be as small as $3.8 \times 10^{-32}$ $cm^6$ $s^{-1}$ which is less than that of $6.1 \times 10^{-32}$ $cm^6$ $s^{-1}$ reported by Guo *et al.* [21]. It is worth noting that the additional nonradiative loss is abscent in the SL-MQWs. All the above results indicate that the luminescence performance of MQWs can be improved significantly by adopting the lattice-matched AlGaN/InGaN superlattices barriers.

In order to understand the luminescence process of the two samples, we have investigate the recombination mechanism at different carrier density. According to the past research, the integral PL intensity $I$ ($Bn^2$) should be a function of excitation density [22], express as

$$I \propto P^F \tag{1}$$

Where $F$ represent the dominant carrier recombination channel at the different carrier density. Assume that the absorption coefficient is a constant, the carrier density ($n$) almost linear increase with the excitation density (kW/$cm^2$). Therefore, the above equation can be expressed as

$$I \propto n^F \tag{2}$$

When $F$ is approaching to 1, the radiative recombination is the main recombination channel. The integral intensity increases linearly with increasing excitation density. When $F$ is approaching to 2, it means that the Shockley-Read-Hall recombination is the main recombination channel [22]. If the value of $F$ is smaller than 1, it means that the dominant recombination channel is Auger recombination or carriers delocalization related nonradiative loss.

The fitting result of the integral intensity $I$ versus $n$ is shown in Fig. 6. At the range of carrier density from $8 \times 10^{16}$ $cm^{-3}$ to $2 \times 10^{18}$ $cm^{-3}$, i.e., region A, the integral intensity of SL-MQWs is less than that of C-MQWs. The value of $F$ of C-MQWs and SL-MQWs are 0.996 and 1.531 respectively. In the C-MQWs, the confinement of carriers by the localized states serve as the radiative center and can make carrier free from the impact of the nonradiative recombination centers [23]. Furthermore, the C-MQWs has a higher V-pits density and the self-screening effect of V-pits can also hinder the carriers from transiting to the defects [24], [25]. However, in the SL-MQWs, the elimination of the misfit strain tend to form a good in-plane uniform MQWs with less spatial compositional fluctuation. The localization effect is weakened and carriers are more easily to transit to the defects for nonradiative recombination. Therefore, although the C-MQWs has higher defect density than the SL-MQWs, the C-MQWs has a higher integral intensity at the carrier density below $2 \times 10^{18}$ $cm^{-3}$.

When the carrier density ranges from $2 \times 10^{18}\,cm^{-3}$ to $10^{19}\,cm^{-3}$, i.e., region B, the value of *F* of C-MQWs and SL-MQWs still are 0.996 and 1.531 respectively. The interesting thing is that the integral intensity of the SL-MQWs surpasses that of C-MQWs, even the carrier recombination in SL-MQWs is still affected by nonradiative recombination centers. That is because the polarization field in SL-MQWs is almost eliminated, resulting in the increasement of the overlap of electrons and holes wave functions. Therefore, despite being influenced by nonradiative recombination, the integral intensity of the SL-MQWs still exceeds that of the C-MQWs.

When the carrier density exceeds $10^{19}\,cm^{-3}$, i.e., region C, the value of *F* of C-MQWs reduced to 0.731. Meanwhile, the FWHM value of the C-MQWs also begin to increase at the high energy side, shown in the Fig. 3(d). These phenomenon are consistent with the observation of Davies *et al.* which the point of onset of droop behavior also correlate with the increase of the PL FWHM [12], [13]. It indicate that a high-order nonradiation recombination channel has been activated in the C-MQWs and results in the droop behavior. Combine with the analysis of the efficiency in Fig. 4(a), a good fit curve by adopting $ABC + kn^m$ model show that except for the Auger recombination, another noradiative loss of carrier also play a role in the droop behavior. However, for the SL-MQWs, the integral intensity increases linearly with increasing excitation density without obvious droop behavior.

Compared with electrical pumping, photoexcitation with the excitation energy below the quantum barriers makes the carriers generated directly in the quantum wells. Therefore, we can exclude the influencing factors such as electron overflow and ineffective holes injection as the reason for efficiency droop at highly excited condition. Moreover, it has been confirmed that the V-pits can build up potential barriers with about several hundreds meV due to the relatively narrow quantum wells of the $(1\bar{1}01)$ sidewalls [24], [25]. These potential barriers will hinder carriers from transiting to the dislocation. And the excited source is pulse laser and the thermal effect can be ignored. Therefore, for the C-MQWs, the V-pits are not likely to be as the nonradiatively centers and result in the efficiency droop [26].

The latest research by Davies *et al.* has shown that both the polar and non-polar InGaN quantum wells structures suffer from the efficiency droop while carrier density exceeds $7 \times 10^{11}\,cm^{-2}\ pulse^{-1}\ QW^{-1}$ [12]. The result shows the elimination of polarized field can not hold back the emergence of droop behavior in quantum wells. And the same droop threshold of the efficiency droop in both polar and non-polar LEDs indicate the droop behavior associate with other carriers delocalization mechanism. According to the recent research, the newest clue related to efficiency droop is the rapidly decaying (ps) transition on the high energy side of the emission spectrum [12], [27], [28], [29]. This transition is occurred between the extended states which can lead to the carrier loss at high excitation carrier density [28]. In our experiment, for the C-MQWs, the onset of the droop behavior relates the broaden of the FWHM and the threshold of carrier density is $10^{19}\,cm^{-3}$. The detail of the droop behavior of the C-MQWs is consistent with the previous reports [12]. Thus, we think the additional nonardiative loss ($kn^m$) in the C-MQWs may associate with the carriers delocalization. For the SL-MQWs, the absence of the droop behavior is probably benefited by the substitution of the AlGaN/InGaN superlattices.

To clarify the extra nonradiative loss of carrier in the C-MQWs, a semiconductor device simulation software, Silvaco ATLAS is employed. The applied band offset ratio of $\triangle E_c \triangle / E_v$ is 0.7:0.3. The induced sheet charge density is assumed to be 40% of the theoretical polarization due to the crystal relaxation through defects during the growth. Through solving Poisson's equation and carrier continuity equation based on a series of physical models implemented in ATLAS software, the band structure of InGaN/GaN QWs and the wavefunction of carriers can be simulated, as shown in the Fig. 7. By considering the spin-orbit coupling effect, the valence band of the QW splits into three sub-bands, as shown in the Fig. 7(a). The valence band offset for the three sub-bands are 292 meV, 132 meV, and 96 meV, respectively. Due to the large polarization field, the quantum well of the valence band transform into triangle potential well which has a weaker confinement effect. Especially for the Valence band#3, the bound state energy of hole exceed the $\triangle E_{v3}$ and transform into the "extended state" [29], as shown in the Fig. 7(a) with blue dash line. Actually, the emission arising from the "extended state", is observed on the industrial-grade green LED in Ref.29.

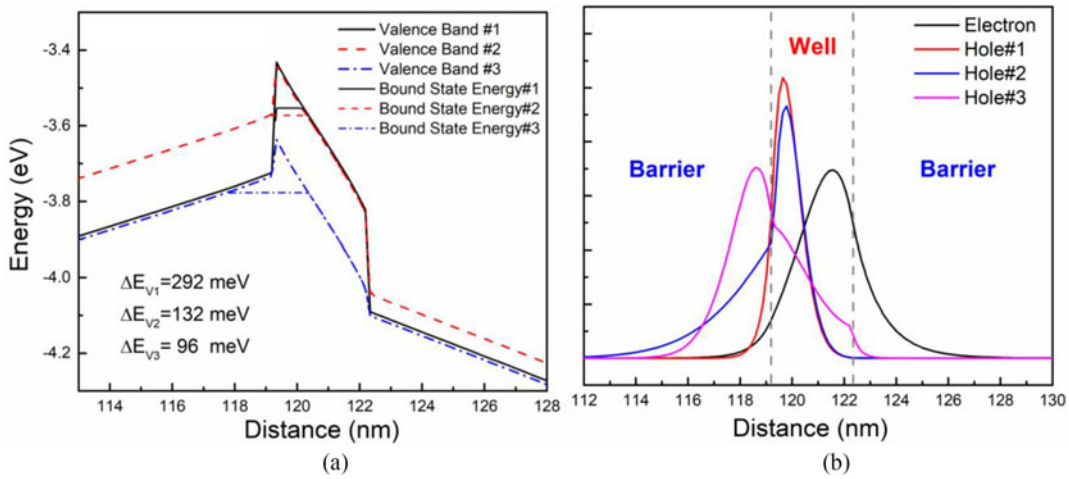


Fig. 7. Simulation result for InGaN/GaN QW, considering the splitting of the valence band. (a) Valence band diagrams and the corresponding bound state energy, (b) the wavefunction of carriers.

Fig. 7(b) shows the wavefunction of carriers with the carrier concentration about $5 \times 10^{19}$ cm$^{-3}$. The wavefunction of the hole confined by the Valence band#3, is mainly distributed in the GaN barriers. And the wavefunction of the hole#2 also has a long trailing into the left GaN barriers. The smaller $\Delta E_{v2}$ and the large polarization field make the confinement of holes weaker and create a new leakage channel for holes to have nonradiative recombination at the defect in the GaN barriers [29]. Therefore, the additional nonradiative loss ($kn^m$) is observed in the C-MQWs. However, the droop behavior is absent in the SL-MQWs sample until the carrier density reaches $10^{20}$ cm$^{-3}$. This may benefit from the AlGaN/InGaN superlattices barriers. The substitution of AlGaN/InGaN superlattices can enlarge the valence band offset and enhance the localization effect of holes in the quantum wells. Moreover, the elimination of polarized field enlarges the overlap of wave function for electrons and holes, and increases the radiative recombination rate. Hence, the efficiency droop does not occur in the SL-MQWs sample.

## 4. Conclusion

In this paper, we fabricate the InGaN/AlGaInN MQWs (SL-MQWs) with lattice-matched AlGaN/InGaN superlattices barriers. The misfit strain is eliminated by the replacement of superlattices. Comparing with the conventional MQWs (C-MQWs), the V-pits density of SL-MQWs reduces to as small as $4.6 \times 10^5$ cm$^{-2}$. The excitation-dependent PL measurement are performed by Ti-sapphire pulse laser with the carrier density up to $2 \times 10^{20}$ cm$^{-3}$. With the increase of carrier density, the stability of the peak wavelength of the SL-MQWs indicate that the polarization field is effectively eliminated by the substitution of the AlGaN/InGaN superlattices. When the carrier density exceeds $10^{19}$ cm$^{-3}$, the efficiency of the C-MQWs droop from 42% to 18%. In spite of the Auger recombination, an additional nonradiative carrier loss with a 2.51-order of the carrier density is exist in the C-MQWs. The SL-MQWs has a slight droop behavior and the Auger coefficient is fitted as small as $3.8 \times 10^{-32}$ cm$^6$ s$^{-1}$. Therefore, we believe the substitution of AlGaN/InGaN superlattices can effective suppress droop behavior and improve the luminescence performance of the MQWs.

## References

[1] S. Nakamura, T. Mukai, and M. Senoh, "Candela-class high-brightness InGaN/AlGaN double-heterostructure blue-light-emitting diodes," *Appl. Phys. Lett.*, vol. 64, no. 13, pp. 1687–1689, 1994.
[2] S. Nakamura *et al.*, "Room-temperature continuous-wave operation of InGaN multi-quantum-well structure laser diodes," *Appl. Phys. Lett.*, vol. 69, no. 26, pp. 4056–4058, 1996.

[3] I. Akasaki, "Nobel lecture: Fascinated journeys into blue light," *Rev. Mod. Phys.*, vol. 87, no. 4, pp. 1119–1131, 2015.
[4] S. Nakamura, "Nobel lecture: Background story of the invention of efficient blue InGaN light emitting diodes," *Rev. Mod. Phys.*, vol. 87, no. 4, pp. 1139–1151, 2015.
[5] G. Verzellesi *et al.*, "Efficiency droop in InGaN/GaN blue light-emitting diodes: Physical mechanisms and remedies," *J. Appl. Phys.*, vol. 114, 2013, Art no. 071101.
[6] J. Cho, E. F. Schubert, and J. K. Kim, "Efficiency droop in light-emitting diodes: Challenges and countermeasures," *Laser Photon. Rev.*, vol. 7, no. 3, pp. 408–421, 2013.
[7] K. Hayashi, T. Yasuda, S. Katsuno, T. Takeuchi, S. Kamiyama, M. Iwaya, and I. Akasaki, "Evaluation of electron overflow in nitride-based LEDs influenced by polarization charges at electron blocking layers," in *Proc. Mater. Res. Soc. Symposia*, vol. 1736, pp. mrsf14-1736–t04-04, 2015.
[8] M.-H. Kim *et al.*, "Origin of efficiency droop in GaN-based light-emitting diodes," *Appl. Phys. Lett.*, vol. 91, 2007, Art no. 183507.
[9] M. F. Schubert *et al.*, "Polarization-matched Ga In N/AlGaInN multi-quantum-well light-emitting diodes with reduced efficiency droop," *Appl. Phys. Lett.*, vol. 93, 2008, Art no. 041102.
[10] H. Y. Ryu, K. S. Jeon, M. G. Kang, H. K. Yuh, Y. H. Choi, and J. S. Lee, "A comparative study of efficiency droop and internal electric field for InGaN blue lighting-emitting diodes on silicon and sapphire substrates," *Sci. Rep.*, vol. 7, 2017, Art no. 44814.
[11] Y. S. Yoo, J. H. Na, S. J. Son, and Y. H. Cho, "Effective suppression of efficiency droop in GaN-based light-emitting diodes: Role of significant reduction of carrier density and built-in field," *Sci. Rep.*, vol. 6, 2016, Art no. 34586.
[12] M. J. Davies *et al.*, "Comparative studies of efficiency droop in polar and non-polar InGaN quantum wells," *Appl. Phys. Lett.*, vol. 108, 2016, Art no. 252101.
[13] M. J. Davies, T. J. Badcock, P. Dawson, M. J. Kappers, R. A. Oliver, and C. J. Humphreys, "High excitation carrier density recombination dynamics of InGaN/GaN quantum well structures: Possible relevance to efficiency droop," *Appl. Phys. Lett.*, vol. 102, 2013, Art no. 022106.
[14] Y. Chen *et al.*, "Pit formation in GaInN quantum wells," *Appl. Phys. Lett.*, vol. 72, pp. 710–712, 1998.
[15] I. H. Kim, H. S. Park, Y. J. Park, and T. Kim, "Formation of V-shaped pits in InGaN/GaN multiquantum wells and bulk InGaN films," *Appl. Phys. Lett.*, vol. 73, pp. 1634–1636, 1998.
[16] S.-N. Lee *et al.*, "Growth and characterization of the AlInGaN quaternary protective layer to suppress the thermal damage of InGaN multiple quantum wells," *J. Cryst. Growth*, vol. 310, pp. 3881–3883, 2008.
[17] G. Xu *et al.*, "Investigation of large Stark shifts in InGaN/GaN multiple quantum wells," *J. Appl. Phys.*, vol. 113, 2013, Art no. 033104.
[18] T. Nagai, T. J. Inagaki, and Y. Kanemitsu, "Band-gap renormalization in highly excited GaN," *Appl. Phys. Lett.*, vol. 84, pp. 1284–1286, 2004.
[19] E. Kuokstis, J. W. Yang, G. Simin, M. A. Khan, R. Gaska, and M. S. Shur, "Two mechanisms of blueshift of edge emission in InGaN-based epilayers and multiple quantum wells," *Appl. Phys. Lett.*, vol. 80, pp. 977–979, 2002.
[20] Y. Sun *et al.*, "Optical excitation study on the efficiency droop behaviors of InGaN/GaN multiple-quantum-well structures," *Appl. Phys. B*, vol. 114, pp. 551–555, 2014.
[21] W. Guo, M. Zhang, P. Bhattacharya, and J. Heo, "Auger recombination in III-nitride nanowires and its effect on nanowire light-emitting diode characteristics," *Nano Lett.*, vol. 11, pp. 1434–1438, 2011.
[22] H. Wang *et al.*, "Influence of excitation power and temperature on photoluminescence in InGaN/GaN multiple quantum wells," *Opt. Exp.*, vol. 20, no. 4, pp. 3932–3940, 2012.
[23] S. F. Chichibu *et al.*, "Origin of defect-insensitive emission probability in In-containing (Al, In, Ga) N alloy semiconductors," *Nature Mater.*, vol. 5, pp. 810–816, 2006.
[24] J. Kim *et al.*, "Influence of V-pits on the efficiency droop in InGaN/GaN quantum wells," *Opt. Exp.*, vol. 22, no. S3, pp. A857–A866, 2014.
[25] A. Hangleiter *et al.*, "Suppression of nonradiative recombination by V-shaped pits in GaInN/GaN quantum wells produces a large increase in the light emission efficiency," *Phys. Rev. Lett.*, vol. 95, 2005, Art no. 127402.
[26] B. Monemar and B. E. Sernelius, "Defect related issues in the "current roll-off" in InGaN based light emitting diodes," *Appl. Phys. Lett.*, vol. 91, 2007, Art no. 181103.
[27] C.-N. Brosseau, M. Perrin, C. Silva, and R. Leonelli, "Carrier recombination dynamics in $In_xGa_{1-x}N$/GaN multiple quantum wells," *Phys. Rev. B*, vol. 82, 2010, Art no. 085305.
[28] G. Sun *et al.*, "Investigation of fast and slow decays in InGaN/GaN quantum wells," *Appl. Phys. Lett.*, vol. 99, 2011, Art no. 081104.
[29] F. Nippert *et al.*, "Polarization-induced confinement of continuous hole-states in highly pumped, industrial-grade, green InGaN quantum wells," *J. Appl. Phys.*, vol. 119, 2016, Art no. 215707.